vessels. Induction of tumor vascular normalization by recombinant apelin administration is difficult because the apelin peptide is unstable. For these reasons, the design of drugs that target the apelin–APJ system, such as more stable and potent APJ receptor agonist, is expected to provide novel agents that by regulating the tumor vasculature will introduce an effective new cancer treatment.

Materials and methods

Mice
C57BL/6 mice, KSN nude mice and BALB/c mice at 8 weeks of age were purchased from Japan SLC (Shizuoka, Japan) and were used between 8 and 12 weeks of age. The animals were housed in environmentally controlled rooms of the animal experimentation facility at Osaka University. All experiments were performed in compliance with the laws and institutional guidelines of Osaka University.

Cells
Cell lines, including colon26, PC3 and LLC, were purchased from RIKEN cell bank (Tsukuba, Japan). The culture medium used was RPMI-1640 containing 10% fetal calf serum, 50 μM 2-mercaptoethanol, 2 mM glutamine and 10 mM HEPES buffer. DCs were grown from bone marrow progenitors in culture medium supplemented with 20 ng/ml recombinant murine granulocyte–macrophage colony-stimulating factor (eBioscience, San Diego, CA, USA) (Fujii *et al.*, 2002). On day 6, αGalCer (100 ng/ml; Kyowa Hakko, Gunma, Japan) was added to immature BMDCs for 40 h. To induce maturation of the DCs, 100 ng/ml lipopolysaccharide (Wako, Osaka, Japan) was added on day 7 for 16 h. Mature αGalCer-pulsed DCs were collected on day 8.

Tissue preparation, immunohistochemistry and flow cytometry
Tissue fixation and staining of sections with antibodies were performed as described previously (Takakura *et al.*, 2000). An anti-CD31 monoclonal antibody (mAb) (BD Biosciences, San Diego, CA, USA), anti-α-smooth muscle actin mAb (Dako, Glostrup, Denmark), anti-apelin mAb (4G5) (Kawamata *et al.*, 2001), anti-APJ polyclonal Ab (Kidoya *et al.*, 2008) and an anti-NKp46 mAb (R&D Systems, Minneapolis, MN, USA) were used for staining. TUNEL (TdT-mediated dNTP nick end labeling) assays were performed using the ApopTag Plus kit (Millipore, Billerica, MA, USA). Sections were observed by conventional microscopy (DM5500 B; Leica, Wetzlar, Germany) or confocal microscopy (TCS/SP5; Leica), and images were acquired with a digital camera (DFC500; Leica). In all assays, an isotype-matched control Ig was used as negative control and it was confirmed that the positive signals were not derived from nonspecific background. Images were processed using the Photoshop CS2 software (Adobe Systems, San Jose, CA, USA). Flow-cytometric analysis was performed as described previously (Yamada and Takakura, 2006). Fluorescence-labeled anti-CD45, anti-CD31, anti-CD86, anti-MHC class-II, anti-TCR-β, anti-CD1d, anti-CD80, anti-CD11c antibody (BD Biosciences) and CD1d tetramer antibodies (Proimmune, Oxford, UK) were used. Stained cells were analyzed with a FACSCalibur (BD Biosciences), by using the FlowJo software (TreeStar, Ashland, OR, USA), and sorted by using a JSAN flow cytometer (Bay Bioscience, Kobe, Japan). Dead cells were excluded from propidium iodide staining or analyses using the two-dimensional profile of the forward versus side scatter.

Real-time PCR analysis
Total RNA was extracted by using the RNeasy plus kit (Qiagen, Hilden, Germany) and reverse-transcribed into cDNA using the ExScript RT-PCR kit (Takara, Otsu, Japan). The primer pairs used for analysis are listed in Supplementary Table 1. Real-time PCR analysis was performed by using Platinum SYBR-Green SuperMix-UDG (Invitrogen, Carlsbad, CA, USA). The levels of PCR products were monitored with an Mx3000P QPCR system (Agilent, Santa Clara, CA, USA). Baseline and threshold were adjusted according to the manufacturer's instructions. The relative abundance of transcripts was normalized to the constitutive expression level of glyceraldehyde-3-phosphate dehydrogenase (GAPDH) RNA.

Tumor growth assay
The mouse *Apelin* gene was cloned into the pCAGSIH expression vector (Kidoya *et al.*, 2008). Colon26 cells and PC3 cells were stably transfected by using the Lipofectamine Plus reagent (Invitrogen) and clones of cells showing stable transfection were obtained by antibiotic resistance selection using G418 (Gibco, Grand Island, NY, USA) and hygromycin-B (Sigma, St Louis, MO, USA). The stably transfected colon26 clones (1×10^6 cells), PC3 clones (1×10^7 cells) or LLC cells (3×10^6 cells) were inoculated subcutaneously into 6- to 8-week-old BALB/c mice, nude mice or C57BL/6 mice, respectively, and tumors were dissected at 12–15 days after implantation. DCs (6×10^5 cells) were administered by intravenous injection 4 days after tumor implantation. To measure hypoxia in tumor tissues, HypoxyProbe-1 (Millipore; 60 mg/kg) was injected intraperitoneally 1 h before killing. Tumors sections were stained using an anti-HypoxyProbe antibody. To evaluate macromolecule infiltration, mice were intravenously injected with fluorescein isothiocyanate-conjugated dextran (500 μg; Vector Laboratories, Burlingame, CA, USA) and dextran was circulated for 10–30 min.

ELISpot assay
IFN-γ-producing cells were analyzed with a mouse IFN-γ ELISpot kit (Mabtech AB, Stockholm, Sweden). Peripheral blood mononuclear cells (5×10^5 per well, 96-well plates) were stimulated by addition of 100 ng/ml αGalCer or vehicle. Concanavalin-A was used as a positive control. IFN-γ spot-forming cells were quantified objectively by using an ImmunoScan computer system and the ImmunoSpot software program (CTL, Cleveland, OH, USA).

Statistical analysis
All data are presented as the means ± s.d. For statistical analysis, the statcel2 software package (OMS, Saitama, Japan) was used, with analysis of variance performed on all data, followed by the Tukey–Kramer multiple comparison test. When only two groups were compared, a two-sided Student's *t*-test was used.

Conflict of interest

The authors declare no conflict of interest.

Acknowledgements

We thank Ms C Takeshita, Ms K Fukuhara and Ms N Fujimoto for technical assistance. *Financial support*: This work

was supported by Grant-in-Aid for Research Activity Start-up (KAKENHI 21890124) from the Japan Society for the Promotion of Science (JSPS) and Research; a grant from the Ministry of Education, Culture, Sports, Science and Technology (MEXT) of Japan; and the YASUDA Medical Foundation.

References

Bergers G, Benjamin LE. (2003). Tumorigenesis and the angiogenic switch. *Nat Rev Cancer* **3**: 401–410.

Bottaro DP, Liotta LA. (2003). Cancer: out of air is not out of action. *Nature* **423**: 593–595.

Brossay L, Chioda M, Burdin N, Koezuka Y, Casorati G, Dellabona P *et al.* (1998). CD1d-mediated recognition of an alpha-galactosylceramide by natural killer T cells is highly conserved through mammalian evolution. *J Exp Med* **188**: 1521–1528.

Cox CM, D'Agostino SL, Miller MK, Heimark RL, Krieg PA. (2006). Apelin, the ligand for the endothelial G-protein-coupled receptor, APJ, is a potent angiogenic factor required for normal vascular development of the frog embryo. *Dev Biol* **296**: 177–189.

Dai T, Ramirez-Correa G, Gao WD. (2006). Apelin increases contractility in failing cardiac muscle. *Eur J Pharmacol* **553**: 222–228.

Dickson PV, Hamner JB, Sims TL, Fraga CH, Ng CY, Rajasekeran S *et al.* (2007). Bevacizumab-induced transient remodeling of the vasculature in neuroblastoma xenografts results in improved delivery and efficacy of systemically administered chemotherapy. *Clin Cancer Res* **13**: 3942–3950.

Dings RP, Vang KB, Castermans K, Popescu F, Zhang Y, Oude Egbrink MG *et al.* (2011). Enhancement of T-cell-mediated antitumor response: angiostatic adjuvant to immunotherapy against cancer. *Clin Cancer Res* **17**: 3134–3145.

Eyries M, Siegfried G, Ciumas M, Montagne K, Agrapart M, Lebrin F *et al.* (2008). Hypoxia-induced apelin expression regulates endothelial cell proliferation and regenerative angiogenesis. *Circ Res* **103**: 432–440.

Fujii S, Shimizu K, Kronenberg M, Steinman RM. (2002). Prolonged IFN-gamma-producing NKT response induced with alpha-galactosylceramide-loaded DCs. *Nat Immunol* **3**: 867–874.

Fukuhara S, Sako K, Minami T, Noda K, Kim HZ, Kodama T *et al.* (2008). Differential function of Tie2 at cell–cell contacts and cell-substratum contacts regulated by angiopoietin-1. *Nat Cell Biol* **10**: 513–526.

Gasparini G, Longo R, Toi M, Ferrara N. (2005). Angiogenic inhibitors: a new therapeutic strategy in oncology. *Nat Clin Pract Oncol* **2**: 562–577.

Gerber HP, Ferrara N. (2005). Pharmacology and pharmacodynamics of bevacizumab as monotherapy or in combination with cytotoxic therapy in preclinical studies. *Cancer Res* **65**: 671–680.

Gerhardt H, Betsholtz C. (2003). Endothelial-pericyte interactions in angiogenesis. *Cell Tissue Res* **314**: 15–23.

Heath VL, Bicknell R. (2009). Anticancer strategies involving the vasculature. *Nat Rev Clin Oncol* **6**: 395–404.

Hurwitz H, Fehrenbacher L, Novotny W, Cartwright T, Hainsworth J, Heim W *et al.* (2004). Bevacizumab plus irinotecan, fluorouracil, and leucovorin for metastatic colorectal cancer. *N Engl J Med* **350**: 2335–2342.

Jain RK. (2005). Normalization of tumor vasculature: an emerging concept in antiangiogenic therapy. *Science* **307**: 58–62.

June CH, Blazar BR, Riley JL. (2009). Engineering lymphocyte subsets: tools, trials and tribulations. *Nat Rev Immunol* **9**: 704–716.

Kakimi K, Guidotti LG, Koezuka Y, Chisari FV. (2000). Natural killer T cell activation inhibits hepatitis B virus replication *in vivo*. *J Exp Med* **192**: 921–930.

Kälin RE, Kretz MP, Meyer AM, Kispert A, Heppner FL, Brändli AW. (2007). Paracrine and autocrine mechanisms of apelin signaling govern embryonic and tumor angiogenesis. *Dev Biol* **305**: 599–614.

Kasai A, Shintani N, Kato H, Matsuda S, Gomi F, Haba R *et al.* (2008). Retardation of retinal vascular development in apelin-deficient mice. *Arterioscler Thromb Vasc Biol* **28**: 1717–1722.

Kasai A, Shintani N, Oda M, Kakuda M, Hashimoto H, Matsuda T *et al.* (2004). Apelin is a novel angiogenic factor in retinal endothelial cells. *Biochem Biophys Res Commun* **325**: 395–400.

Kawamata Y, Habata Y, Fukusumi S, Hosoya M, Fujii R, Hinuma S *et al.* (2001). Molecular properties of apelin: tissue distribution and receptor binding. *Biochim Biophys Acta* **1538**: 162–171.

Kawano T, Cui J, Koezuka Y, Toura I, Kaneko Y, Motoki K *et al.* (1997). CD1d-restricted and TCR-mediated activation of valpha14 NKT cells by glycosylceramides. *Science* **278**: 1626–1629.

Kawano T, Nakayama T, Kamada N, Kaneko Y, Harada M, Ogura N *et al.* (1999). Antitumor cytotoxicity mediated by ligand-activated human V alpha24 NKT cells. *Cancer Res* **59**: 5102–5105.

Kidoya H, Naito H, Takakura N. (2010). Apelin induces enlarged and nonleaky blood vessels for functional recovery from ischemia. *Blood* **115**: 3166–3174.

Kidoya H, Ueno M, Yamada Y, Mochizuki N, Nakata M, Yano T *et al.* (2008). Spatial and temporal role of the apelin/APJ system in the caliber size regulation of blood vessels during angiogenesis. *EMBO J* **27**: 522–534.

Kim KJ, Li B, Winer J, Armanini M, Gillett N, Phillips HS *et al.* (1993). Inhibition of vascular endothelial growth factor-induced angiogenesis suppresses tumour growth *in vivo*. *Nature* **362**: 841–844.

Kunii N, Horiguchi S, Motohashi S, Yamamoto H, Ueno N, Yamamoto S *et al.* (2009). Combination therapy of *in vitro*-expanded natural killer T cells and alpha-galactosylceramide-pulsed antigen-presenting cells in patients with recurrent head and neck carcinoma. *Cancer Sci* **100**: 1092–1098.

Lago F, Dieguez C, Gomez-Reino J, Gualillo O. (2007). The emerging role of adipokines as mediators of inflammation and immune responses. *Cytokine Growth Factor Rev* **18**: 313–325.

Lambrecht NW, Yakubov I, Zer C, Sachs G. (2006). Transcriptomes of purified gastric ECL and parietal cells: identification of a novel pathway regulating acid secretion. *Physiol Genomics* **25**: 153–165.

Lohela M, Bry M, Tammela T, Alitalo K. (2009). VEGFs and receptors involved in angiogenesis versus lymphangiogenesis. *Curr Opin Cell Biol* **21**: 154–165.

Masri B, Morin N, Cornu M, Knibiehler B, Audigier Y. (2004). Apelin (65-77) activates p70 S6 kinase and is mitogenic for umbilical endothelial cells. *FASEB J* **18**: 1909–1911.

Motohashi S, Nagato K, Kunii N, Yamamoto H, Yamasaki K, Okita K *et al.* (2009). A phase I–II study of alpha-galactosylceramide-pulsed IL-2/GM-CSF-cultured peripheral blood mononuclear cells in patients with advanced and recurrent non-small cell lung cancer. *J Immunol* **182**: 2492–2501.

Nieda M, Nicol A, Koezuka Y, Kikuchi A, Lapteva N, Tanaka Y *et al.* (2001). TRAIL expression by activated human CD4(+)V alpha 24NKT cells induces *in vitro* and *in vivo* apoptosis of human acute myeloid leukemia cells. *Blood* **97**: 2067–2074.

Nieda M, Okai M, Tazbirkova A, Lin H, Yamaura A, Ide K *et al.* (2004). Therapeutic activation of Valpha24+Vbeta11+ NKT cells in human subjects results in highly coordinated secondary activation of acquired and innate immunity. *Blood* **103**: 383–389.

Padera TP, Stoll BR, Tooredman JB, Capen D, di Tomaso E, Jain RK. (2004). Pathology: cancer cells compress intratumour vessels. *Nature* **427**: 695.

Rosenberg SA, Lotze MT, Yang JC, Aebersold PM, Linehan WM, Seipp CA *et al.* (1989). Experience with the use of high-dose interleukin-2 in the treatment of 652 cancer patients. *Ann Surg* **210**: 474–484; discussion 484–475.

Rosenberg SA, Restifo NP, Yang JC, Morgan RA, Dudley ME. (2008). Adoptive cell transfer: a clinical path to effective cancer immunotherapy. *Nat Rev Cancer* **8**: 299–308.

Seaman S, Stevens J, Yang MY, Logsdon D, Graff-Cherry C, St Croix B. (2007). Genes that distinguish physiological and pathological angiogenesis. *Cancer Cell* **11**: 539–554.

Seino K, Fujii S, Harada M, Motohashi S, Nakayama T, Fujisawa T *et al.* (2005). Valpha14 NKT cell-mediated antitumor responses and their clinical application. *Springer Semin Immunopathol* **27**: 65–74.

Shin T, Nakayama T, Akutsu Y, Motohashi S, Shibata Y, Harada M *et al.* (2001). Inhibition of tumor metastasis by adoptive transfer of IL-12-activated Valpha14 NKT cells. *Int J Cancer* **91**: 523–528.

Singh AK, Wilson MT, Hong S, Olivares-Villagomez D, Du C, Stanic AK *et al.* (2001). Natural killer T cell activation protects mice against experimental autoimmune encephalomyelitis. *J Exp Med* **194**: 1801–1811.

Smyth MJ, Crowe NY, Pellicci DG, Kyparissoudis K, Kelly JM, Takeda K *et al.* (2002). Sequential production of interferon-gamma by NK1.1(+) T cells and natural killer cells is essential for the antimetastatic effect of alpha-galactosylceramide. *Blood* **99**: 1259–1266.

Sorhede Winzell M, Magnusson C, Ahren B. (2005). The apj receptor is expressed in pancreatic islets and its ligand, apelin, inhibits insulin secretion in mice. *Regul Pept* **131**: 12–17.

Sorli SC, Le Gonidec S, Knibiehler B, Audigier Y. (2007). Apelin is a potent activator of tumour neoangiogenesis. *Oncogene* **26**: 7692–7699.

Spada FM, Koezuka Y, Porcelli SA. (1998). CD1d-restricted recognition of synthetic glycolipid antigens by human natural killer T cells. *J Exp Med* **188**: 1529–1534.

Steinman RM, Banchereau J. (2007). Taking dendritic cells into medicine. *Nature* **449**: 419–426.

Takakura N, Watanabe T, Suenobu S, Yamada Y, Noda T, Ito Y *et al.* (2000). A role for hematopoietic stem cells in promoting angiogenesis. *Cell* **102**: 199–209.

Taniguchi M, Harada M, Kojo S, Nakayama T, Wakao H. (2003). The regulatory role of Valpha14 NKT cells in innate and acquired immune response. *Annu Rev Immunol* **21**: 483–513.

Tatemoto K, Hosoya M, Habata Y, Fujii R, Kakegawa T, Zou MX *et al.* (1998). Isolation and characterization of a novel endogenous peptide ligand for the human APJ receptor. *Biochem Biophys Res Commun* **251**: 471–476.

Willett CG, Kozin SV, Duda DG, di Tomaso E, Kozak KR, Boucher Y *et al.* (2006). Combined vascular endothelial growth factor-targeted therapy and radiotherapy for rectal cancer: theory and clinical practice. *Semin Oncol* **33**: S35–S40.

Yamada Y, Takakura N. (2006). Physiological pathway of differentiation of hematopoietic stem cell population into mural cells. *J Exp Med* **203**: 1055–1065.

Supplementary Information accompanies the paper on the Oncogene website (http://www.nature.com/onc)

European Journal of Radiology 81 (2012) 1134–1139

Contents lists available at ScienceDirect

European Journal of Radiology

journal homepage: www.elsevier.com/locate/ejrad

Usefulness of contrast-enhanced three-dimensional MR angiography using time-resolved imaging of contrast kinetics applied to description of Extracranial Arteriovenous Malformations: Initial Experience

Hiroki Higashihara[a,*], Keigo Osuga[a], Takashi Ueguchi[b], Hiromitsu Onishi[a], Hisashi Tanaka[a], Noboru Maeda[a], Kaname Tomoda[a], Noriyuki Tomiyama[a]

[a] Department of Diagnostic and Interventional Radiology, Osaka University Graduate School of Medicine, 2-2 Yamadaoka, Suita, Osaka 565-0871, Japan
[b] Department of Radiology, Osaka University Hospital, 2-2 Yamadaoka, Suita, Osaka 565-0871, Japan

ARTICLE INFO

Article history:
Received 1 November 2010
Received in revised form 5 March 2011
Accepted 11 March 2011

Keywords:
MR angiography
Contrast media
Vascular anomalies
Arteriovenous malformation

ABSTRACT

Purpose: The purpose of this study was to evaluate the usefulness of contrast-enhanced three-dimensional MR angiography using time-resolved imaging of contrast kinetics (TRICKS-MRA) to demonstrate extracranial arteriovenous malformations (E-AVMs).
Materials and methods: TRICKS-MRA was performed in 33 patients (adults; $n=30$, children; $n=3$) with E-AVMs. Four different scan protocols were arranged based on the size of E-AVM, and serial images were acquired from the start of contrast injection with a time frame ranging from 1.2 to 7.1 s. Demonstration of feeding arteries and drainage veins, and the extent of nidus was qualitatively graded using a three-point scale. In sixteen patients who underwent DSA 3 days to 15 months after TRICKS-MRA, the comparability of TRICKS-MRA to DSA was evaluated using a three-point scale. In each category, score of 3 or excellent was defined as the positive result.
Results: Demonstration of the feeding arteries, the drainage veins, and the extent of nidus were graded as excellent in 68%, 65%, and 58% of the patients, respectively. Comparability of TRICKS-MRA to DSA was excellent in 75%, 88%, and 88% of the sixteen patients who underwent DSA.
Conclusion: TRICKS-MRA is a feasible and useful vascular imaging technique to provide time-resolved analysis of angioarchitecture of E-AVMs.

1. Introduction

Extracranial vascular anomalies are seen in children or young adults and are often difficult to properly diagnose and treat [1,2]. Since 1996, practical classification of vascular anomalies has been developed by the International Society for the Study of the Vascular Anomalies (ISSVA) [3]. According to the ISSVA classification, vascular anomalies are mainly divided into two categories: hemangiomas and vascular malformations. Recognition of the clinical and imaging features of each type of vascular anomaly is important, and vascular imaging studies are essential to define their anatomic extent [1,2,4,5]. Digital subtraction angiography (DSA) has been an essential vascular imaging for the diagnosis and peri-operative assessment of extracranial arteriovenous malformations (E-AVMs). However, the catheter angiography is invasive, and has similar risks of contrast-induced nephrotoxicity and radiation exposure by contrast-enhanced CT imaging [6,7]. Thus, minimally invasive vascular imaging without radiation exposure is of great demand for morphological and hemodynamic evaluation and proper treatment planning of E-AVMs. MR angiography (MRA) is less invasive because it evokes no radiation exposure and can avoid the use of potentially nephrotoxic iodinated contrast agents. Therefore, it is anticipated that MRA can supplant DSA, as the vascular imaging of choice for primary evaluation of E-AVMs [8–12]. In order to visualize clearly and identify accurately the feeding artery, nidus and drainage vein, sufficient temporal resolution is necessary for MRA because E-AVMs are fast-flow lesions. Several techniques have been developed for vascular imaging by MRA. Time of flight (TOF), phase-contrast and contrast-enhanced magnetic resonance angiography (MRA) produce static images of AVMs and suffer from T1 shortening artifacts from hemoglobin breakdown products. Furthermore, TOF-MRA is insensitive to slow flow because of the saturation effects. Two- (2D) or three-dimensional (3D) dynamic contrast enhanced time-resolved MRA overcomes these limitations, and have demonstrated a good correlation with DSA in the evaluation of intracranial AVM [13–15]. Compared with 2D acquisition, 3D dynamic contrast enhanced time-resolved MRA is superior in spatial resolution, partial volume artifacts, signal-to-noise ratio (SNR)

* Corresponding author. Tel.: +81 6 6879 3434; fax: +81 6 6879 3439.
E-mail address: h-higashihara@radiol.med.osaka-u.ac.jp (H. Higashihara).

0720-048X/$ – see front matter.
doi:10.1016/j.ejrad.2011.03.040

Table 1
The location of E-AVMs.

Location of AVMs		Number of patients
Head and neck		11
Upper extremity	Overall	12
	Hand	7
	Forearm	2*
	Arm	2*
	Shoulder	2
Lower extremity	Overall	9
	Foot	4
	Calf	0
	Thigh	5
Trunk		1
Total		33

Note: *One patient had a diffuse AVM extending from the arm to forearm.

and volume coverage [16]. One means of improving the spatial resolution is TR strategy of key-hole imaging technique, such as time-resolved imaging of contrast kinetics (TRICKS), in which the center of k-space is oversampled, whereas higher k-space is undersampled. Because of increased temporal resolution of TRICKS-MRA, the diagnostic capability has been improved for the analysis of intracranial AVMs [17,18] and peripheral arterial occlusive diseases [19,20]. To the best of our knowledge, there has been no report regarding the demonstration of E-AVMs using this MRA technique. The purpose of this study was to evaluate the feasibility and usefulness of TRICK-MRA imaging for the analysis of E-AVMs.

2. Materials and methods

2.1. Patient population

Institutional review board approval waived the requirement of written informed consent for this retrospective study. Between February 2005 and July 2007, thirty-one patients who were clinically suspected of having E-AVM were included in this study. The locations of the E-AVMs were shown in Table 1. Mean age was 36 years old (range 2–66 years). Three patients were pediatric cases under eighteen years old. DSA was performed in 16 patients 3 days to 15 months after MRA, because endovascular treatment was considered. Of 16 patients, 8 patients subsequently underwent transcatheter or direct puncture embolotherapy, and the remaining eight patients were followed up without treatment. All patients gave their informed consent to undergo the contrast-enhanced MRA, DSA and additional treatment.

2.2. MR technique

The time-resolved contrast-enhanced 3D MRA with TRICKS sequence was obtained using a 1.5T-MR scanner (Signa Excite HD, GE Healthcare, Milwaukee, WI) equipped with surface coils (8ch neurovascular array coil, 12ch peripheral vascular array coil, 3ch shoulder array coil, 8ch body array coil, 8ch CTL spine array coil, GP flex coil and quadrature knee coil). TRICKS-MRA acquires multiple 3D volumes during the passage of the contrast agent bolus by using time-resolved acquisition [17,21]. With such acquisition, the repeated sampling of the critical central k-space views is combined with temporal interpolation to produce a series of time-resolved 3D images [17]. Time-resolved acquisitions such as TRICKS-MRA obviate timing tests [17,21,22] and the separate acquisition of precontrast images for mask mode subtraction [23]. In our institution, parallel imaging technique for improvement of temporal resolution could not be applied to TRICKS-MRA during the period of this study.

Because the location and size of E-AVMs were variable, four different scan protocols (Protocol Large, Middle, Small and Tiny) were prepared for TRICKS-MRA (Table 2). Among them, suitable scan protocol was selected individually in each case. The minimum temporal resolution was 1.2 s for hand AVMs, and the maximum one was 7.1 s for thigh AVMs (mean temporal resolution: 3.0 s). Temporal resolution with each scan protocol was shown in Table 2.

Image acquisition was started at the same time as the start of the intravenous administration of contrast media. The scan time was 180 s for the lower extremity lesions and 120 s for the remaining lesions. A typical injection protocol consisted of bolus injection of 20 ml of Gd-DTPA (Magnevist; Bayer Schering Pharma, Berlin, Germany) at 2.0 ml/s followed by flushing with 20 ml of saline at 2.0 ml/s. For pediatric cases younger than 18 years old, the dose of Gd-DTPA was reduced to 0.3 ml/kg body weight.

Especially for cases with the head and neck lesions, the lateral projection was preferred as the basic view, because it gave a better separation of the external carotid artery branches (Fig. 1A–C). To avoid overlapping of the contra-lateral side branches in the lateral projection, and to reduce the slab thickness to shorten the time frame, MRA images of the right and left half of the face were sequentially acquired by injecting half the amount of contrast material separately. The minimal overlap of the both sides of the face was secured in the middle of the face.

3. Image assessment

Two radiologists, one with eight and the other with eighteen years of experience in diagnosis and endovascular treatment for vascular anomalies qualitatively analyzed TRICKS-MRA images by consensus. The degree to which TRICKS-MRA could demonstrate the feeding arteries, the drainage veins, and the extent of the nidus was assessed by using a 3-point scale scores: 3 – excellent (clearly visible), 2 – fair (moderately visible), 1 – poor (poorly visible). In addition, in sixteen patients who underwent DSA, how comparable the findings of TRICKS-MRA were to detect each of the feeding arteries, the drainage veins, and the extent of nidus was assessed by using 3-point scale scores: 3 – excellent (very comparable), 2 – fair (moderately comparable), 1 – poor (poorly comparable). In case of head and neck lesions, only images of the affected side were evaluated for these assessments. The score of 3 was considered as the positive result, and the proportion of the patients scored 3 was calculated in each assessment.

Table 2
Scan protocols of TRICKS-MRA according to the lesion size.

Protocol	TR/TE (ms)	Flip angle (°)	Slice thickness (mm)	Matrix	FOV (cm)	Slab thickness (mm)	Temporal resolution (s)
Large	2.2–3.5/0.7–1.2	20/35	3–10	320 × 160–320 × 224	36 × 36–48 × 34	120–192	2.2–7.1
Middle	2.3–2.9/0.8–1.1	20	6–8	288 × 160	22 × 24–36 × 36	84–192	1.8–3.7
Small	3.1–3.3/0.9–1	20	5	256 × 160	18 × 18–22 × 22	90–100	2.2–4
Tiny	3.1–3.8/0.9–1.1	20–45	3–5	256 × 160–320 × 224	16 × 12–26 × 18	50–79	1.2–3.2

Note: TRICKS = time-resolved imaging of contrast kinetics, FOV = field of view.

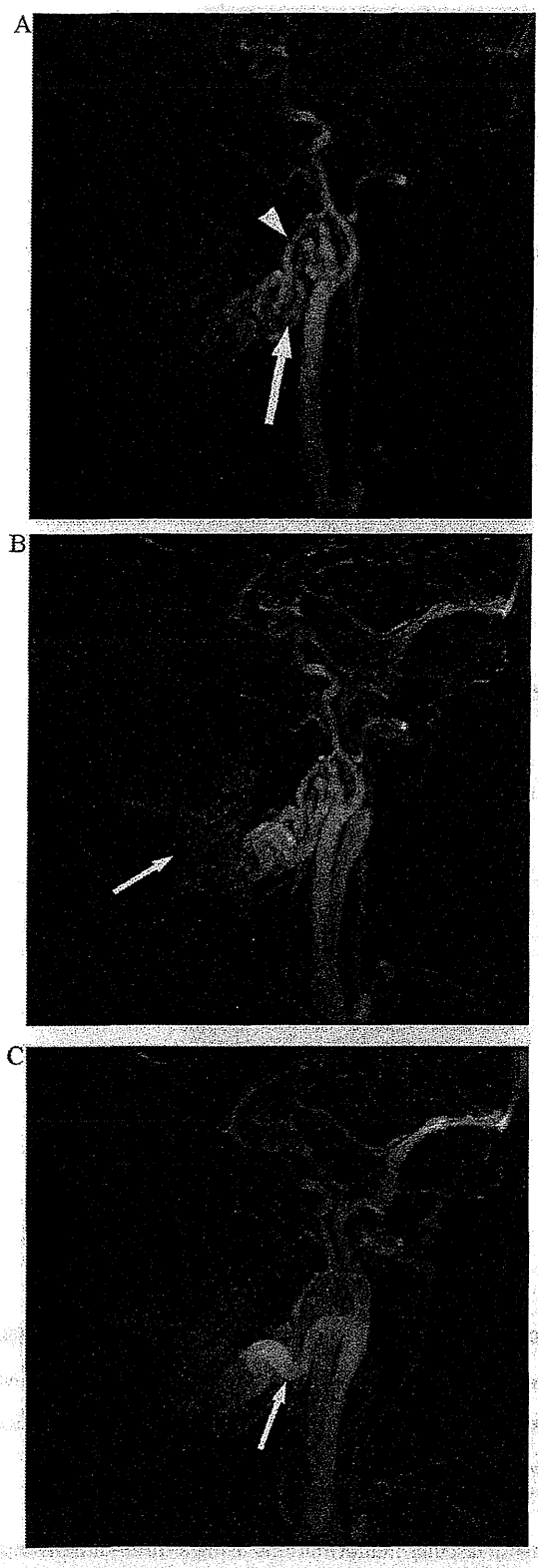

Fig. 1. A 33-year-old woman with AVM of the tongue.
(Sequence parameters of TRICKS-MRA: Temporal Resolution: 2.5 s TR: 3.2/TE: 1, Flip Angle: 20°, Slice Thickness: 5 mm, Slice Spacing 2.5 mm, Matrix: 256 × 160, FOV: 22 × 22, Slab Thickness: 90 mm, type of shown image: MIP image.)
(A) TRICKS-MRA of the right face shows AVM in the tongue in the lateral view. Demonstration of both the pure arterial image and the feeding arteries were graded as excellent. The right lingual artery (arrow) and facial artery (arrow head) were clearly shown as feeding arteries (7 of 25 phases). (B) The extent of nidus was clearly delineated in the subsequent phase (arrow) (8 of 25 phases). It was also graded as excellent. (C) The drainage vein was shown in the venous phase (arrow).

Table 3
Assessment of demonstration of E-AVMs by TRICKS-MRA.

Category	Image score
Protocol	3/2/1
The feeding arteries	21/7/3
Large	2/4/2
Middle	2/2/0
Small	10/0/1
Tiny	7/1/0
The drainage veins	20/7/4
Large	6/2/0
Middle	2/2/0
Small	6/1/4
Tiny	6/2/0
The extent of nidus	18/10/3
Large	1/5/2
Middle	2/1/1
Small	9/2/0
Tiny	6/2/0

4. Results

TRICKS-MRA could be achieved in all cases. The several initial frames did not show any enhanced vessel because of the difference in the arrival time of the contrast material among the locations.

4.1. Image assessment

The results of assessment for each category per scan protocol are shown in Table 3. To visualize the feeding arteries (Figs. 1A and 2A), 21 of 31 patients (68%) was graded as excellent, and 3 of 31 patients (10%) was graded as poor. Two of the three patients had diffuse and extensive lesions in the forearm to the humerus, and the scan protocol of Large was used. However, the blood flow was too fast to demonstrate the feeding arteries clearly, and they were overlapped with diffuse spread of the nidus and dilated drainage veins. The similar findings were verified by additional DSA. In the remaining one patient with a tiny lesion in the nasal root, the scan protocol of Small was used, but the feeding artery was extremely fine on DSA. To visualize the draining veins (Fig. 1C), 20 patients (65%) were graded as excellent, and four patients (13%) were graded as poor. All the four patients had small AVMs in the medial face or head including the nasal root, lip and occipital region. As the nidus was small or fine, the drainage vein was not dilated, and difficult to be shown clearly. To visualize the extent of nidus (Fig. 1D), 18 patients (58%) were graded as excellent, and three patients (10%) were graded as poor. These three patients had large ill-defined diffuse AVMs in the forearm to humerus (the same patients as above in the feeding artery) and the thigh, and the scan protocol of Large and Middle were used in two and one patients, respectively. As a result, the extent of nidus was difficult to be shown clearly in these patients (Fig. 3).

4.2. Comparability of TRICKS-MRA to DSA

The results of comparability of TRICKS-MRA to DSA are shown in Table 4. 75%, 88%, and 88% of the patients were graded as excellent to show the feeding arteries, the drainage veins, and the extent of nidus, respectively. Two to three patients with the nasal root or thigh lesions as described before were graded as poor for each component.

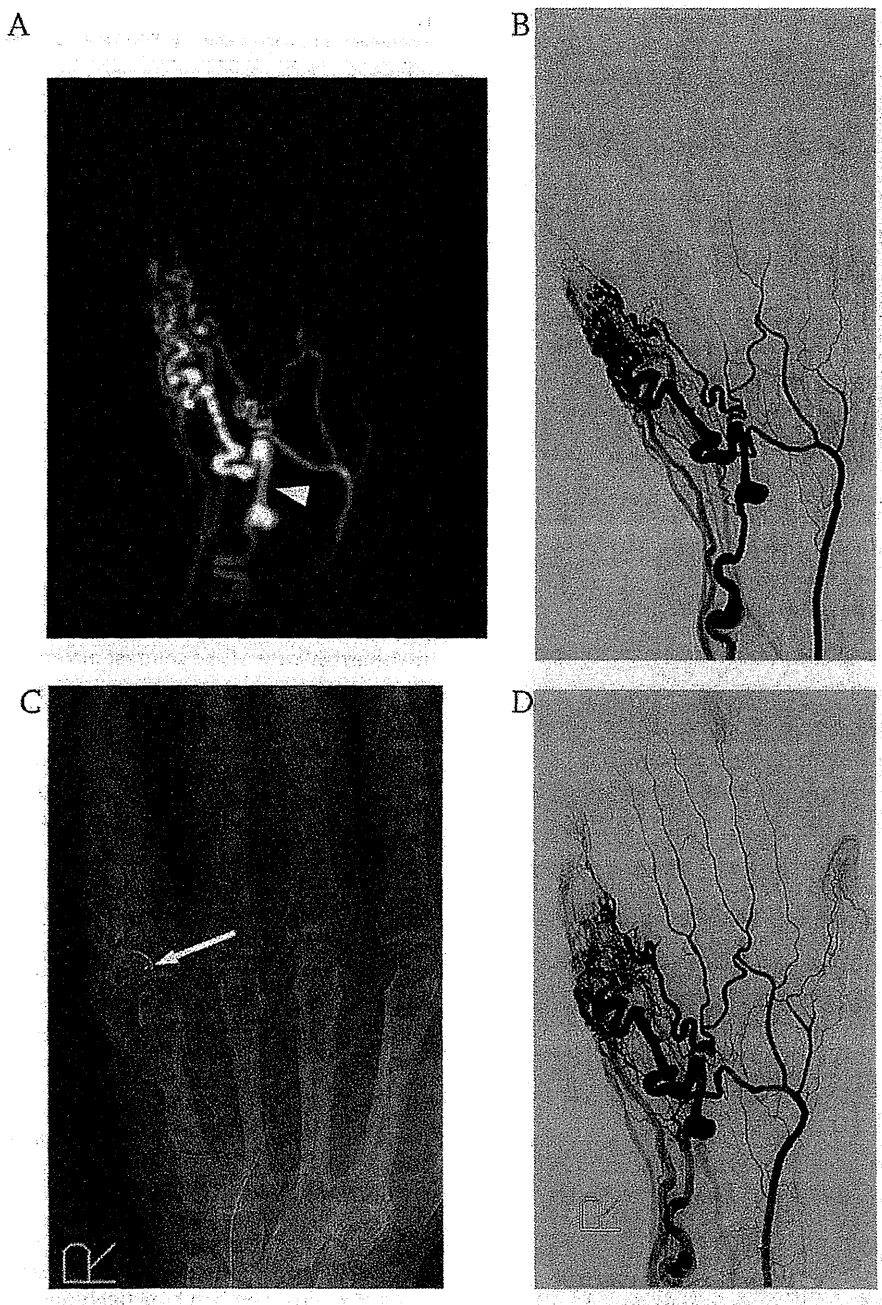

Fig. 2. A 26-year-old woman with AVM of the left fifth finger.
(Sequence parameters of TRICKS-MRA: Temporal Resolution: 1.2 s TR: 3.6/TE: 1.1, Flip Angle: 20°, Slice Thickness: 4.2 mm, Slice Spacing 2.1 mm, Matrix: 256 × 160, FOV: 16 × 12, Slab Thickness: 42 mm, type of shown image: MIP image.)
(A) TRICKS-MRA showed the infiltrative nidus supplied by a dominant tortuous feeding artery (arrow head). This was important anatomical information for planning transcatheter embolotherapy.
(B) Embolization was performed, and the finding of DSA correlated well with that of TRICKS-MRA. The correlation of the finding between TRICKS-MRA and DSA was graded as good.
(C) A small thin microcatheter was advanced selectively into the nidus, and dehydrated ethanol was carefully injected (arrow).
(D) After embolization, opacity of the nidus was reduced, while visualization of digital arteries was improved.

5. Discussion

MR imaging is helpful for the classification of vascular anomalies and for defining their anatomic extent [24]. However, both spatial and temporal resolutions of conventional MRA have been still limited for evaluating vascular components and hemodynamics of each lesion [24]. Herborn et al. [25] first reported the efficacy of time-resolved contrast-enhanced dynamic MRA for assessment of peripheral vascular malformations using a three-dimensional fast low-angle shot sequence. However, the sequence required a separate bolus test injection to determine the arrival time of contrast media into the feeding artery, and still, the images were obtained only at approximately every 30 s interval. In contrast, the mean temporal resolution was significantly improved to approximately 3–5 s in our study and also similar second-scale in other studies by applying the novel technique like TRICKS [17,19]. In addition, there

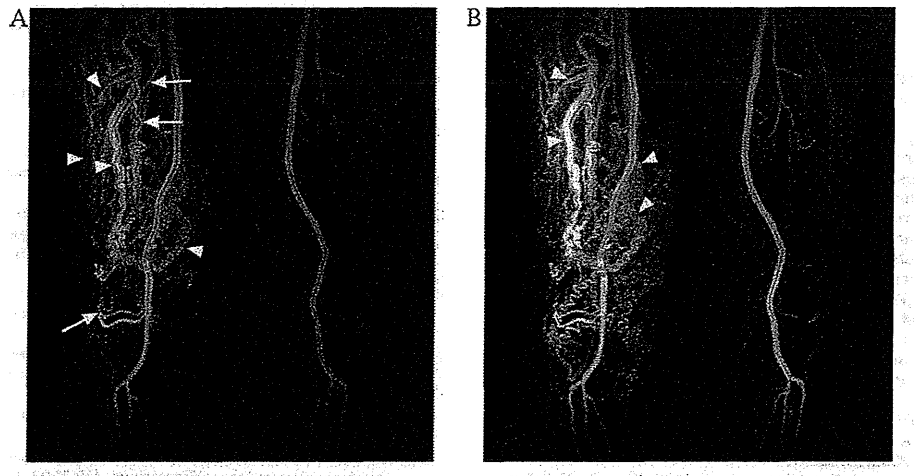

Fig. 3. A 60-year-old man with AVM of the right thigh.
(Sequence parameters of TRICKS-MRA: Temporal Resolution: 7.1 s TR: 3.5/TE: 1, Flip Angle: 35°, Slice Thickness: 3 mm, Slice Spacing 1.5 mm, Matrix: 320 × 224, FOV: 44 × 30.8, Slab Thickness: 150 mm, type of shown image: MIP image.)
(A) TRICKS-MRA shows AVM in the right thigh. The right superficial femoral artery (arrow) was recognized as a feeding artery overlapped with drainage veins (arrow head).
(B) The drainage veins (arrow head) were more prominent in the subsequent phase (6 of 30 phases).

Table 4
Comparability of TRICKS-MRA to DSA.

Category	Score 3/2/1
The feeding artery	12/1/3
The drainage vein	14/0/2
The extent of nidus	14/0/2

The definition of 3-point scale scores: 3 – excellent (TRICKS-MRA was very comparable to DSA), 2 – fair (moderately comparable), 1 – poor (poorly comparable).

is no need for test-injection or operator-dependent triggering to obtain pure arterial images.

In the image assessment, demonstration of the feeding arteries, the drainage veins, and the extent of nidus were graded as excellent in 68%, 65% and 58% of the patients, respectively. In contrast, the visualization were poor especially in extensive AVM, in which the feeding arteries overlapped the dilated drainage veins and diffuse spread of the nidus in the same time frames. In such large E-AVMs, TRICKS-MRA requires the thicker slab thickness for the wide coverage of the lesion, however, temporal resolution is compromised instead. During the study period, parallel imaging technique to improve temporal resolution of TRICKS-MRA was not available in our MRI equipment. If this technique were applied in TRICKS-MRA, the demonstration of each component might be improved especially in larger E-AVMs. In comparison with DSA, TRICKS-MRA showed the comparable findings with DSA in 75%, 88%, and 88% of the patients to show the feeding arteries, drainage veins, and the extent of nidus, respectively. Therefore, TRICKS-MRA is a feasible and useful modality prior to DSA and the further endovascular treatments in selected patients with E-AVMs. TRICKS-MRA may reduce the needs for routine catheter angiography of diagnostic purpose especially in children and young adults.

Our study has several limitations. First, it was a retrospective study with a small number of patients enrolled. E-AVM is an uncommon disease that can occur in the entire body. As the location and size of each lesion significantly differ among patients, the comprehensive image assessment is difficult. Nevertheless, this is the first report assessing the feasibility of TRICKS-MRA to demonstrate E-AVMs in spite of the small patient group. Second, the temporal resolution of TRICKS-MRA was still inadequate compared with that of DSA to assess E-AVMs. Because the temporal resolution in 3D MRA inversely correlates with spatial resolution, it is difficult to ensure a short time frame to obtain sufficient slab thickness. Therefore, in this study, we prepared the four different scan protocols according to the size and location of E-AVMs (Table 2). However, the time frame could be shortened to less than 2 s only in small thin objects like a hand, whereas it increased to as long as 6–7 s in large thick lesions. Especially, in the thigh and trunk lesions requiring large scan coverage, it was necessary to increase slab and slice thickness to minimize the temporal resolution. At this time, it is still early to recommend particular appropriate parameters through our limited experience in this study. Petkova et al. reported the effectiveness of TRICKS-MRA combining parallel imaging for the diagnosis and follow-up of intracranial AVMs [26]. The combination of parallel imaging technique and TRICKS-MRA is promising to improve the temporal resolution and image quality in the assessment of E-AVMs. Further investigation will be necessary to optimize scan parameters and the method of contrast injection according to the type and location of each anomaly.

In conclusion, although there are several limitations, TRICKS-MRA is a feasible and useful vascular imaging technique to provide time-resolved analysis of angioarchitecture of E-AVMs.

Conflicts of interest

The authors or authors' institutions have no conflicts of interest associated with this study. This includes financial or personal relationships that inappropriately influence (bias) his actions (such relationships are also known as dual commitments, competing interests, or competing loyalties) within 3 years of the work beginning submitted.

References

[1] Hyodoh H, Hori M, Akiba H, et al. Peripheral vascular malformations: imaging, treatment approaches, and therapeutic issues. RadioGraphics 2005;25(Suppl. 1):S159–171.
[2] Dubois J, Soulez G, Oliva VL, et al. Soft-tissue venous malformations in adult patients: imaging and therapeutic issues. RadioGraphics 2001;21:1519–31.
[3] Enjolras O. Classification and management of the various superficial vascular anomalies: hemangiomas and vascular malformations. J Dermatol 1997;24:701–10.
[4] Enjorlas O, Mulliken JB. The current management of vascular birthmarks. Pediatr Dermatol 1993;10:311–33.
[5] Jackson IT, Carreno R, Potparic Z, Hussain K. Hemangiomas, vascular malformations, and lymphovenous malformations: classification and methods of treatment. Plast Reconstr Surg 1993;91:1216–30.
[6] Loewe C, Schoder M, Rand T, et al. Peripheral vascular occlusive disease: evaluation with contrast-enhanced moving-bed MR angiography versus

digital subtraction angiography in 106 patients. AJR Am J Roentgenol 2002;179:1013–21.
[7] Vavrik J, Rohrmoser GM, Madani B, et al. Comparison of MR angiography versus digital subtraction angiography as a basis for planning treatment of lower limb occlusive disease. J Endovasc Ther 2004;11:294–301.
[8] Cohen JM, Weinreb JC, Redman HC. Arteriovenous malformations of the extremities: MR imaging. Radiology 1986;158:475–9.
[9] Meyer JS, Hoffer FA, Barnes PD, Mulliken JB. Biological classification of soft-tissue vascular anomalies: MR correlation. AJR 1991;157:559–64.
[10] Huch Boni RA, Brunner U, Bollinger A, et al. Management of congenital angiodysplasia of the lower limb: magnetic resonance imaging and angiography versus conventional angiography. Br J Radiol 1995;68:1308–15.
[11] Baker LL, Dillon WP, Hieshima GB, et al. Hemangiomas and vascular malformations of the head and neck: MR characterization. AJNR 1993;14:307–14.
[12] Rak KM, Yakes WF, Ray RL, et al. MR imaging of symptomatic peripheral vascular malformations. AJR 1992;159:107–12.
[13] Warren DJ, Hoggard N, Walton L, et al. Cerebral arteriovenous malformations: comparison of novel magnetic resonance angiographic techniques and conventional catheter angiography. Neurosurgery 2001;48:973–82, discussion 982–983.
[14] Coley SC, Romanowski CA, Hodgson TJ, Griffiths PD. Dural arteriovenous fistulae: noninvasive diagnosis with dynamic MR digital subtraction angiography. AJNR Am J Neuroradiol 2002;23:404–7.
[15] Mori H, Aoki S, Okubo T, et al. Two-dimensional thick-slice MR digital subtraction angiography in the assessment of small to medium-size intracranial arteriovenous malformations. Neuroradiology 2003;45:27–33.
[16] Coley SC, Wild JM, Wilkinson ID, Griffiths PD. Neurovascular MRI with dynamic contrast-enhanced subtraction angiography. Neuroradiology 2003;45:843–50.
[17] Korosec FR, Frayne R, Grist TM, Mistretta CA. Time-resolved contrast-enhanced 3D MR angiography. Magn Reson Med 1996;36:345–51.
[18] Reinacher PC, Stracke P, Reinges MH, Hans FJ, Krings T. Contrastenhanced time-resolved 3-D MRA: applications in neurosurgery and interventional neuroradiology. Neuroradiology 2007;49(Suppl. 1):S3–13.
[19] Swan JS, Carroll TJ, Kennell TW, et al. Time-resolved three-dimensional contrast-enhanced MR angiography of the peripheral vessels. Radiology 2002;225:43–52.
[20] Wang CC, Liang HL, Hsiao CC, et al. Single-dose time-resolved contrast enhanced hybrid MR angiography in diagnosis of peripheral arterial disease: compared with digital subtraction angiography. J Magn Reson Imaging 2010;32:935–42.
[21] Schoenberg SO, Bock M, Knopp MV, et al. Renal arteries: optimization of three-dimensional gadolinium-enhanced MR angiography with bolus-timing-independent fast multiphase acquisition in a single breath hold. Radiology 1999;211:667–79.
[22] Carroll TJ, Korosec FR, Petermann GM, Grist TM, Turski PA. Carotid bifurcation: evaluation of time-resolved three-dimensional contrast-enhanced MR angiography. Radiology 2001;220:525–32.
[23] Frayne R, Grist T, Swan JS, et al. 3D MR DSA: effects of injection protocol and image masking. J Magn Reson Imaging 2000;12:476–87.
[24] Dobson MJ, Hartley RW, Ashleigh R, Watson Y, Hawnaur JM. MR angiography and MR imaging of symptomatic vascular malformations. Clin Radiol 1997;52:595–602.
[25] Herborn CU, Goyen M, Lauenstein TC, et al. Comprehensive time-resolved MRI of peripheral vascular malformations. AJR 2003;181:729–35.
[26] Petkova M, Gauvrit JY, Trystram D, et al. Three-dimensional dynamic time-resolved contrast-enhanced MRA using parallel imaging and a variable rate k-space sampling strategy in intracranial arteriovenous malformations. J Magn Reson Imaging 2009;29:7–12.

Interactive CardioVascular and Thoracic Surgery 14 (2012) 665-667
doi:10.1093/icvts/ivs024 Advance Access publication 20 February 2012

CASE REPORT

Successful lobectomy for central large pulmonary arteriovenous malformation

Takashi Kanou[a], Yasushi Shintani[a,*], Keigo Osuga[b] and Meinoshin Okumura[a]

[a] Department of General Thoracic Surgery, Osaka University Graduate School of Medicine, Osaka University, Osaka, Japan
[b] Department of Diagnostic and Interventional Radiology, Osaka University Graduate School of Medicine, Osaka, Japan

* Corresponding author. Department of General Thoracic Surgery, Osaka University Graduate School of Medicine, Osaka University, 2-2-L5 Yamadaoka, Suita, Osaka 565-0871, Japan. Tel: +81-6-68793152; fax: +81-6-68793164; e-mail: yshintani@thoracic.med.osaka-u.ac.jp (Y. Shintani).

Received 10 November 2011; received in revised form 3 January 2012; accepted 10 January 2012

Abstract

A pulmonary arteriovenous malformation (PAVM) is caused by abnormal communications between the pulmonary arteries and veins. In this study, a 64-year old woman presented with a large PAVM in the central upper lobe of the right lung. As feeding vessels were large and short, the patient was scheduled for resection therapy. By clamping the right main pulmonary artery, the blood flow into the PAVM was controlled and lobectomy was performed safely. Although advances in interventional radiology have led to the introduction of obliterative techniques, surgical resection is still an effective first option for patients with a large, centrally located PAVM.

Keywords: Arteriovenous malformation · Pulmonary · Thoracic surgery

INTRODUCTION

A pulmonary arteriovenous malformation (PAVM) is caused by abnormal communications between the pulmonary arteries and veins [1]. This malformation has a right-to-left shunt and induces chronic hypoxaemia, paradoxical embolism or infection. A large, centrally located PAVM with aneurysmal formation is uncommon and the optimal treatment remains unclear [2].

CASE REPORT

A 64-year old woman with a PAVM in the upper lobe of the right lung, initially discovered several decades ago, was referred to our hospital with recently developed symptoms including dyspnoea on exertion, cyanosis, polycythemia and right cardiac failure. There was no family history of hereditary haemorrhagic telangiectasia. Significant clinical findings included central cyanosis and digital clubbing. The laboratory results included a low systemic arterial oxygen saturation (SaO_2) of 65% and a haemoglobin level of 20.4 g/dl. Chest radiography revealed a lobulated mass in the upper right lung, and chest computed tomography (CT) showed a 10 × 8-cm nodular lesion centrally located in the upper lobe of the right lung (Fig. 1a). A pulmonary angiogram confirmed the lesion to be a PAVM supplied by feeding arteries 8 mm in diameter and 1.5 cm in length before entering the venous sac (Fig. 1b). The shunt fraction was calculated as 53% by a whole-body scan with technetium-99m-labelled macroaggregated albumin particles.

The patient underwent a right anterolateral thoracotomy. Findings at surgery included a dilated superior pulmonary vein (Supplementary Video 1; Fig. 1c) and a large pulsating complex PAVM, which nearly completely occupied the right upper lobe. The PAVM was supplied by the superior trunk of the right pulmonary artery. To avoid damaging the weakened vessel walls, we clamped the right main pulmonary artery and controlled the blood flow into the PAVM (Fig. 1d). Restriction of the blood flow into the right upper lobe significantly reduced the diameters of both superior trunks and superior vein, which allowed for safe stapling (Fig. 1e and f). Furthermore, SaO_2 improved from 63 to 100% immediately after clamping the right pulmonary artery (Table 1). Pathologically, a cystic structure with an irregular lumen and anastomosing vascular channels was noted. The postoperative course was uneventful. A follow-up examination at 1-year showed no cyanosis or dyspnoea on exertion, and room air arterial blood gas oxygen saturation of 98%.

DISCUSSION

Transcatheter embolization, which involves blocking of the artery that leads to the PAVM with metallic coils or detachable balloons, is the treatment of choice and most lesions can be successfully managed [3, 4]. However, failures of transcatheter embolization for PAVMs occur more often in aneurysms with large and short feeding vessels because of a high risk of inadvertent coil migration as well as a significant instability of the guiding catheter during coil deployment [5]. Georghiou *et al.* [6] reported that, in the presence of a large solitary malformation, centrally located, surgery is still a safe and effective option. In the present case, after considering both the vessel diameter and length, interventional therapy was thought to be inappropriate as treatment.

Recently, video-assisted thoracoscopy has been used during resection of a small PAVM [4]. In the present case,

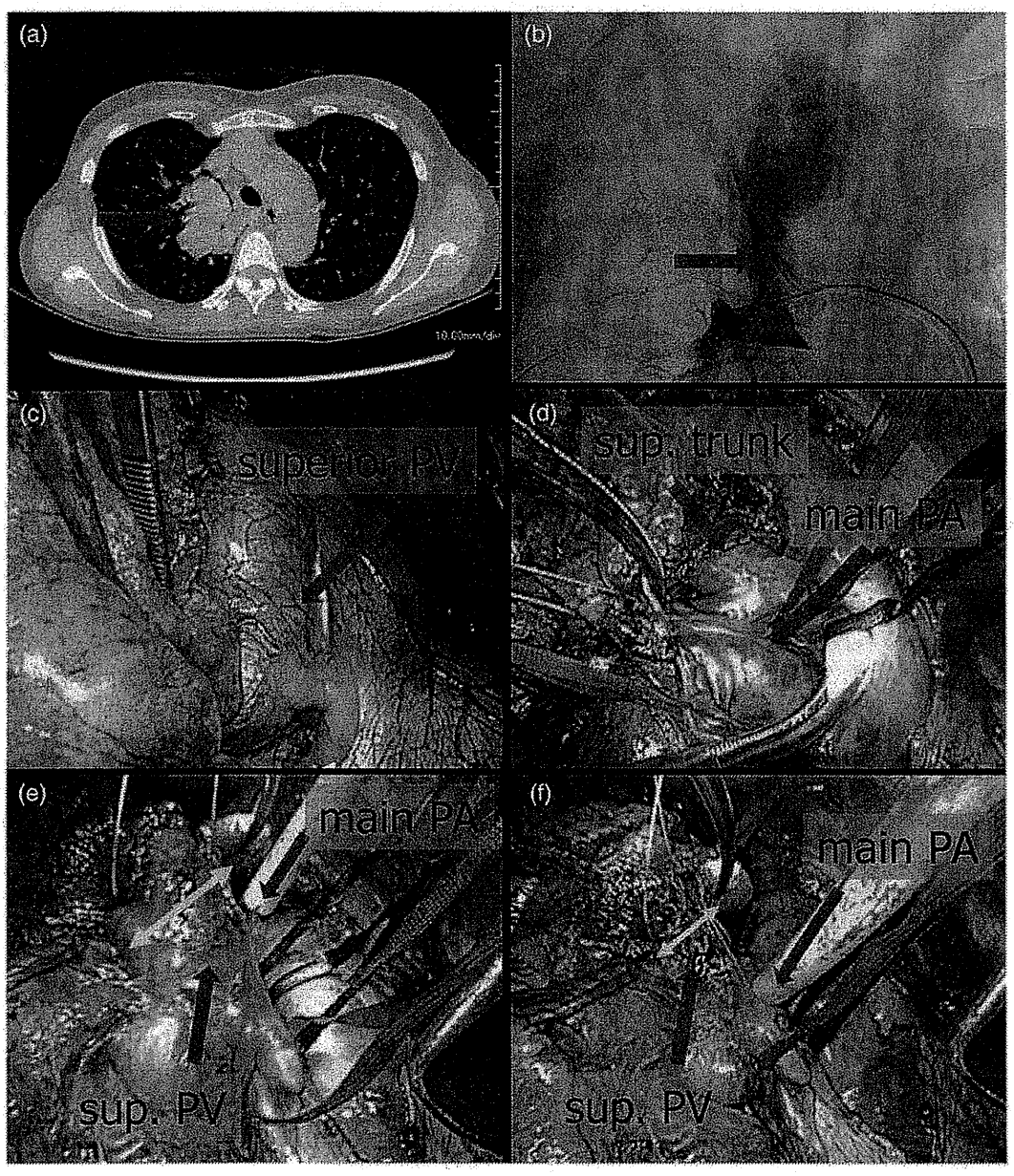

Figure 1: (**a**) Chest CT scan showing arteriovenous fistula (arrows). (**b**) Pulmonary angiography showing pulmonary arteriovenous malformation located in the right upper lobe with the short length of the feeding artery before entering the venous sac (arrow). (**c**) Photograph of operative field. Dilated superior pulmonary vein. (**d**) Main pulmonary artery and dilated superior trunk of the right pulmonary artery. (**e**) Dilated superior pulmonary vein before clamping of main pulmonary artery (yellow arrow). (**f**) Collapsed superior pulmonary vein after clamping of main pulmonary artery. Blocking blood flow to the right main pulmonary artery significantly reduced the diameter of the superior pulmonary vein (yellow arrow).

Table 1: Perioperative arterial blood gas (ABG)

	FiO_2 (%)	pH	pCO_2 (mmHg)	PO_2 (mmHg)
Preoperative (baseline)	Room air	7.39	34.1	41.0
Intraoperative preresection	100	7.28	51.9	55.4
Intraoperative postresection	100	7.29	50.1	400
Postoperative (POD 7)	Room air	7.39	34.6	75.9

the large size (8 cm in diameter) and the position near the hilum implied that the blood flow into the PAVM was extremely high. In addition, some investigators have proposed that the cause is a defect in the terminal arterial loops [7], which causes enlargement of thin-walled capillary sacs, indicating that the feeding vessels as well as aneurysm sac might be fragile. Therefore, we used a muscle-sparing thoracotomy approach to achieve better hilar and vascular control. In addition, we considered that there was potential for damage to the pulmonary artery or pulmonary vein

Supplementary Video 1: A dilated superior pulmonary vein was seen at the hilar region of the right upper lobe. To avoid damaging the weakened vessel walls, we clamped the right main pulmonary artery and controlled the blood flow into the PAVM. Restriction of the blood flow into the right upper lobe significantly reduced the diameters of both superior trunks and superior vein, which allowed for safe stapling the superior vein (V1–3) and superior trunk of the right pulmonary artery.

during transection of those vessels, therefore we blocked the blood flow into the PAVM before shearing off the vessels. Using this method, a right upper lobectomy was safely performed.

In conclusion, we report a case of a large PAVM with aneurysmal formation located in the pulmonary hilum. Surgical treatment still plays an important role when managing such large, high-flow PAVMs with aneurysmal formation in a central location.

SUPPLEMENTARY MATERIAL

Supplementary material is available at *ICVTS* online.

Conflict of interest: none declared.

REFERENCES

[1] Khurshid I, Downie GH. Pulmonary arteriovenous malformation. Postgrad Med J 2002;78:191–7.
[2] Hsu PK, Hsu WH, Wu YC. Central large pulmonary arteriovenous malformation with aneurysmal dilatation. Thorac Cardiovasc Surg 2009;57:434–6.
[3] Pollak JS, Saluja S, Thabet A, Henderson KJ, Denbow N, White RI Jr. Clinical and anatomic outcomes after embolotherapy of pulmonary arteriovenous malformations. J Vasc Interv Radiol 2006;17:35–44.
[4] Gupta P, Mordin C, Curtis J, Hughes JM, Shovlin CL, Jackson JE. Pulmonary arteriovenous malformations: effect of embolization on right-to-left shunt, hypoxemia, and exercise tolerance in 66 patients. AJR Am J Roentgenol 2002;179:347–55.
[5] Tal MG, Saluja S, Henderson KJ, White RI Jr. Vein of Galen technique for occluding the aneurysmal sac of pulmonary arteriovenous malformations. J Vasc Interv Radiol 2002;13:1261–4.
[6] Georghiou GP, Berman M, Vidne BA, Saute M. Pulmonary arteriovenous malformation treated by lobectomy. Eur J Cardiothorac Surg 2003;24:328–30.
[7] Watanabe N, Munakata Y, Ogiwara M, Miyatake M, Nakagawa F, Hirayama J. A case of pulmonary arteriovenous malformation in a patient with brain absess successfully treated with video-assisted thoracoscopic resection. Chest 1995;108:1724–7.

ISSVA分類とその臨床的意義

三村秀文* 松井裕輔* 藤原寛康** 平木隆夫**
郷原英夫** 宗田由子* 道下宣成* 木股敬裕*** 金澤 右**

体表の血管腫・血管奇形は稀な疾患で、疾患概念と治療法に混乱が見られる。近年ISSVA分類に基づいて診断を行い、治療方針を決定することが国際的に標準化しつつある。ISSVA分類の利点は、わかりやすい世界共通の病名を用いて血管腫と血管奇形を区別することにより、適切な臨床診断と治療方針を導くことにある。

Key words: ISSVA分類, 血管奇形, 血管腫

はじめに

体表の血管腫・血管奇形(総称してvascular anomalies)は全身のあらゆる部位に発症し、その発生部位により担当する診療科は多岐にまたがり、疾患概念と治療法に混乱が見られる。従来から血管腫・血管奇形の分類には慣用的用語を含め、さまざまな名称が使用されており、混乱の大きな原因となっている。近年、ISSVA(the International Society for the Study of Vascular Anomalies)分類(表1)[1]に基づいて表在の血管腫・血管奇形の診断を行い、治療方針を決定することが国際的に標準化しつつある。ISSVA分類の利点は、なるべく単純でわかりやすい世界共通の病名を用いて血管腫と血管奇形を区別することにより、適切な臨床診断と治療方針を導くことにある。ISSVA分類の啓蒙・普及が待ち望まれている。

1 ISSVA分類の必要性

体表の血管腫と血管奇形は異なる疾患であり、治療法が異なる。血管腫の中で頻度の高い乳児血管腫は生後急速に増大し、幼児期に徐々に退縮する病変であり、通常治療を要さない。一方、血管奇形は自然退縮することはなく、疼痛・潰瘍・出血・感染・患肢の成長異常、機能障害、整容上の問題などを来し、しばしば治療を要する。その原因の多くは明らかではない。

血管奇形をもつ患者の中には、血管腫と診断され、いずれ縮小するといわれ放置され治療困難な状態まで増大したり、血管奇形に効果のない放射線治療を施行され発育障害を来したり、また最近では乳児血管腫に対する有効性が報告されているβブロッカーを投与されていたりなど、誤った診療をされるケースは少なくない。

さらに、血管奇形の診断がついても、効果的な治療法・治療指針は未確立である。従来、保存的治療・外科的切除が行われてきたが、近年、機能・形態の温存が可能なinterventional radiology(IVR)、すなわち硬化療法・塞栓術が新しい治療として普及し、国際的に標準治療となりつつある。しかしながら、これらはわが国においては多くが保険適応ではな

* Mimura H., Matsui Y., Souda Y., Michishita N.　川崎医科大学附属川崎病院放射線科　** Fujiwara H., Hiraki T., Gobara H., Kanazawa S.　岡山大学病院放射線科　*** Kimata Y.　同形成外科

表1　血管腫・血管奇形のISSVA分類(Enjolrasらによる改訂)

Vascular tumors	Vascular malformations
Infantile hemangiomas	**Slow-flow vascular malformations:**
Congenital hemangiomas (RICH and NICH)	Capillary malformation (CM)
Tufted angioma (with or without Kasabach-Merritt syndrome)	Port-wine stain
Kaposiform hemangioendothelioma (with or without Kasabach-Merritt syndrome)	Telangiectasia
Spindle cell hemangioendothelioma	Angiokeratoma
Other, rare hemangioendotheliomas (epithelioid, composite, retiform, polymorphous, Dabska tumor, lymphangioendotheliomatosis, etc.)	Venous malformation (VM)
Dermatologic acquired vascular tumors (pyogenic granuloma, targetoid hemangioma, glomeruloid hemangioma, microvenular hemangioma, etc.)	Common sporadic VM
	Bean syndrome
	Familial cutaneous and mucosal venous malformation (VMCM)
	Glomuvenous malformation (GVM) (glomangioma)
	Maffucci syndrome
	Lymphatic malformation (LM)
	Fast-flow vascular malformations:
	Arterial malformation (AM)
	Arteriovenous fistula (AVF)
	Arteriovenous malformation (AVM)
	Complex-combined vascular malformations:
	CVM, CLM, LVM, CLVM, AVM-LM, CM-AVM

C：capillary，V：venous，L：lymphatic，AV：arteriovenous，M：malformation，RICH：rapidly involuting congenital hemangioma，NICH：noninvoluting congenital hemangioma
(文献1)より転載)

い．さらに，血管奇形には，病変が小さく切除治療が可能なものから，多発性あるいは巨大で一肢全体に及ぶなど切除不能・治療抵抗性の病変が少なくない．後者には長期にわたり患者のQOLを深刻に損なう難治性の病態が含まれる．診断のコンセンサス形成，病態の解明，治療法の開発は急務である．

2 ISSVA分類の概要

血管腫・血管奇形の国際学会であるthe International Society for Study of Vascular Anomalies (ISSVA)は，16年間の隔年開催のワークショップを行った後1992年に発足し，学際的かつ国際的な協力を基に，疾患の理解を深め，マネージメントを改善することを主要目的としてきた．"angiomas"や"vascular birthmarks(血管性母斑)"の多様な医学用語は，長きにわたり患者の治療に関与するさまざまな専門家の間で障害になっていたため，ISSVAではこれらの古い用語を使用しないことを決めた．1996年の学術会議で採択されたISSVA分類[2]はきわめて根本的な分類体系であり，共通の用語を提供した．

この体系は，1982年に発表されたMullikenとGlowackiの研究[3]に基づいている．彼らは病理組織所見に基づいて，血管病変を血管性腫瘍(血管腫など)と血管奇形の2つに区別した．血管性腫瘍は細胞(主に内皮)の腫瘍性増殖を来し発育する．非常によく見られる乳児血管腫は良性の血管性腫瘍である．その一方，血管奇形では内皮細胞のturnoverは正常であり，形態形成の局所的な異常と考えられ，すなわち杯形成・脈管形成を制御する経路の機能障害により引き起こされたと考えられる．

血管性腫瘍の末尾に付け加えられる"oma(腫瘍)"は腫瘍細胞の増殖を意味し，したがって，"angioma""hemangioma""lymphangioma"を血管奇形に用いるのは誤っている．血管性腫瘍はそのタイプにより退縮または存続する．血管奇形は退縮せず，未治療であれば生涯存続する．それらのほとんどは小児期に成長に比例して増大し，治療しなければ経時的に悪化するものがある．血管性腫瘍と血管奇形の識別は臨床的，放射線学的，病理学的特徴と罹患率だけでなく，それらの治療法が全く違うことも非常に重要である．乳児血管腫と血管奇形との主な相違点

表2　乳児血管腫と血管奇形の主な相違点

	乳児血管腫	血管奇形
発症時期および経過	幼小児期	治療しなければ生涯続く
経過	3期（増殖期，退縮期，退縮後）	成長に比例して増大／少しずつ増大
男：女	1：3～9	1：1
細胞	内皮細胞のturnover亢進	内皮細胞のturnover正常
	肥満細胞数の増加	肥満細胞数正常
	厚い基底膜	薄い基底膜
増大の起点	ない（あるいは不明）	外傷，ホルモンの変化
病理	増殖期，退縮期，退縮後に特徴的な像	CM，VM，LM，AVMそれぞれの特徴
	GLUT-1＋	GLUT-1－
MRI	flow voidを伴う境界明瞭な腫瘤	VM，LMはT2強調像で高信号
		AVMはflow void
治療	自然退縮，薬物治療，手術，レーザー	病変に応じてレーザー，手術，塞栓術，硬化療法など

GLUT-1：glucose transporter-1
（文献1）より転載）

肉眼所見

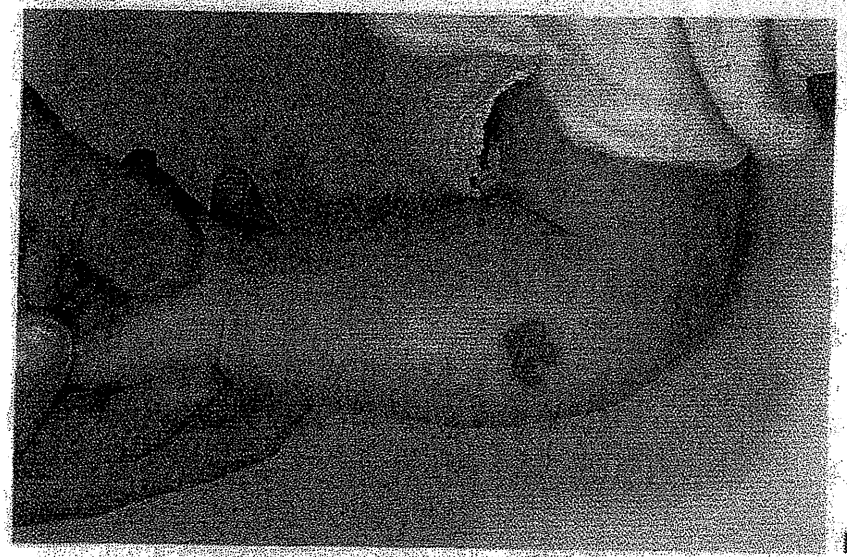

図1　乳児血管腫（局面型）

を表2[1]に示す．

血管性腫瘍と血管奇形を分けることに加えて，さらに血行動態と優位な異常脈管に基づく血管奇形の細分類も作成された．血管奇形は低流速（slow-flow）か高流速（fast-flow）かであり，前者は毛細血管奇形（capillary malformation：CM），静脈奇形（venous malformation：VM），リンパ管奇形（lymphatic malformation：LM），後者は動静脈奇形（arteriovenous malformation：AVM）に細分類される．これは非常に重要である．それらのマネージメントは診断と治療のいずれに関してもサブタイプによって異なるからである．一部の患者は複合の混合型血管奇形を有し，capillary venous malformation（CVM），capillary lymphatic malformation（CLM），capillary lymphatic venous malformation（CLVM），lymphatic venous malformation（LVM）などと呼ばれる（表1）．

3 血管性腫瘍と血管奇形

1）血管性腫瘍

a. 乳児血管腫（infantile hemangioma）

乳児血管腫は幼児期に最も多い腫瘍で，血管内皮

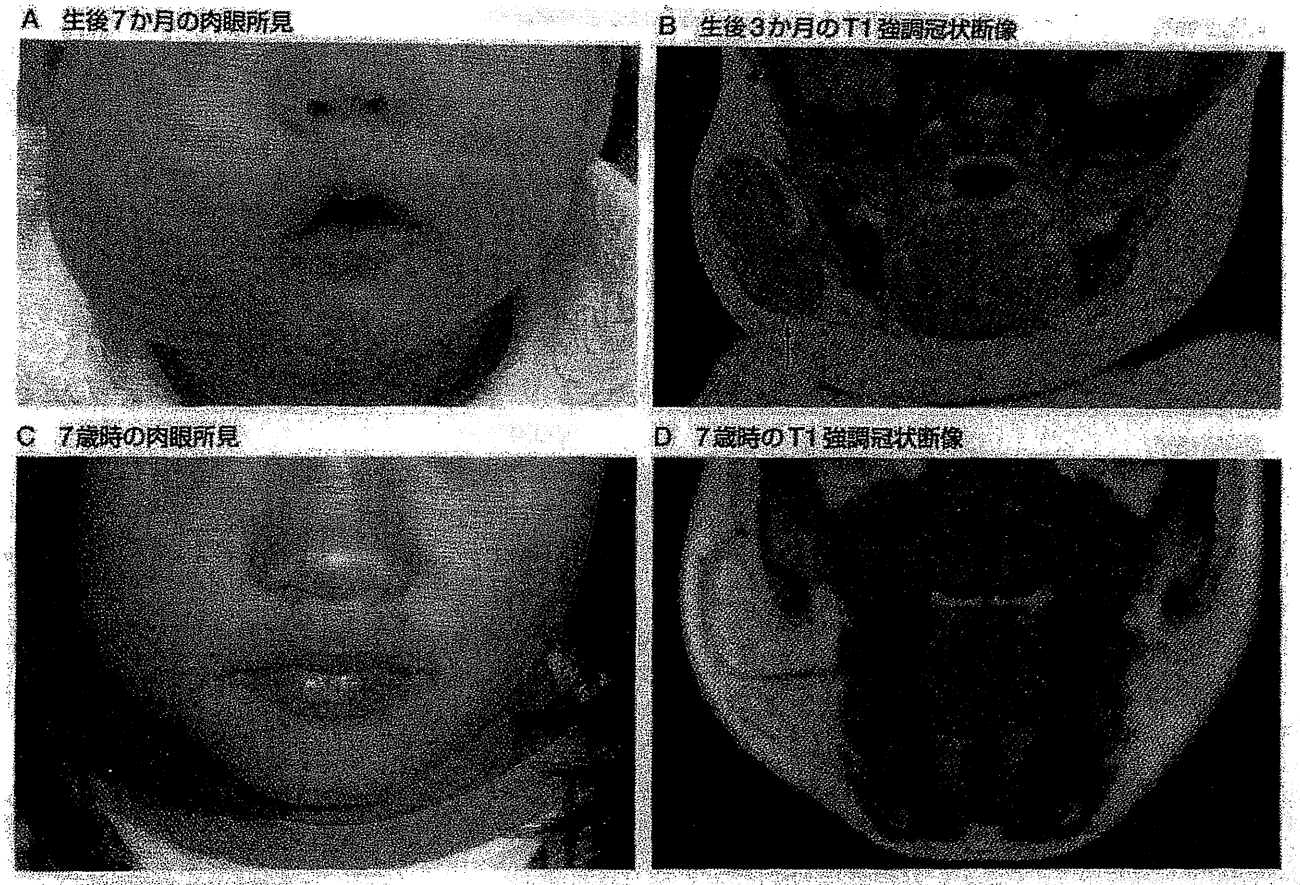

図2 乳児血管腫(皮下型)
A：右頬部の腫脹が見られる.
B：右頬部皮下脂肪織内に低信号を呈する腫瘤が見られる(→).
C：腫脹は改善している.
D：腫瘤は脂肪組織に置換されている.

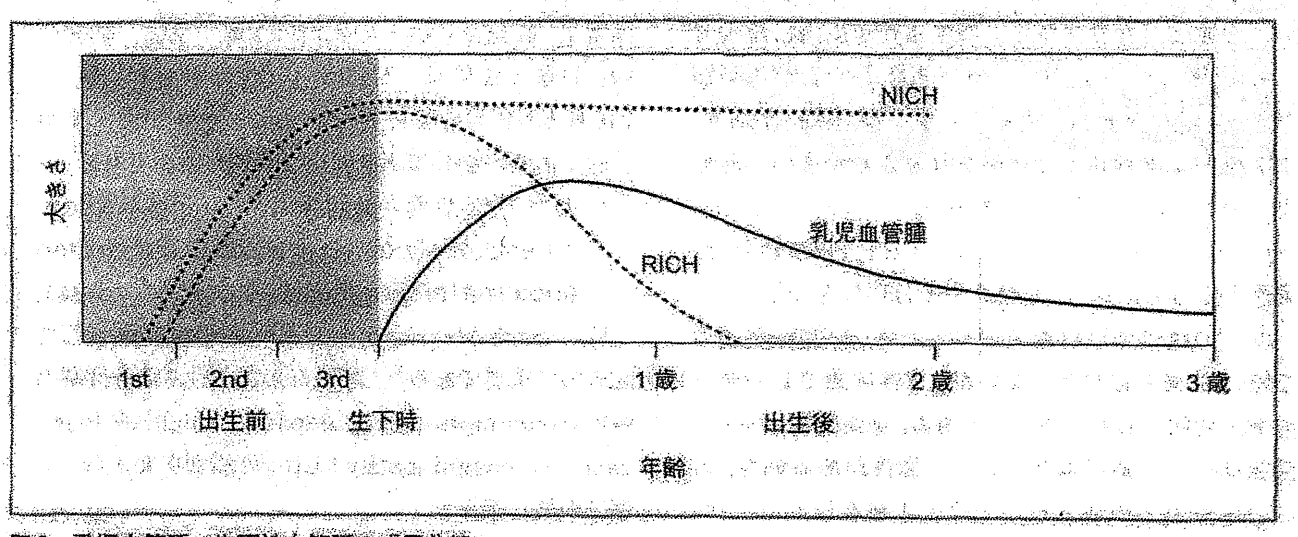

図3 乳児血管腫・先天性血管腫の成長曲線
RICH：rapidly involuting congenital hemangioma
NICH：noninvoluting congenital hemangioma
(文献6)より転載)

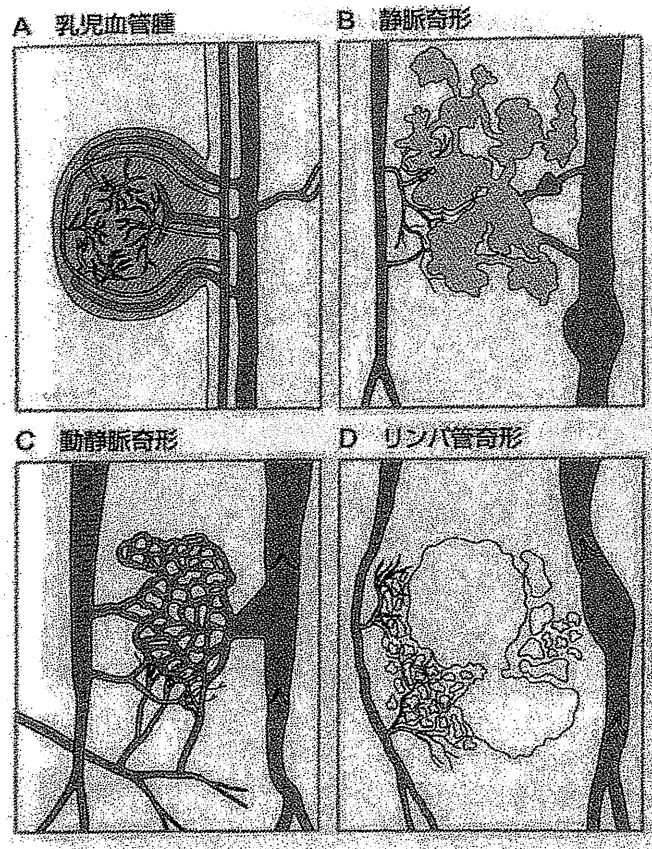

図4 乳児血管腫・血管奇形のシェーマ
A：多血性腫瘍の形態を呈する．
B：異常な静脈腔の拡張からなる．
C：毛細血管が欠損し，異常な血管網が置き換わっている．
D：拡張した異常なリンパ管からなる．
(文献8)より転載)

細胞の腫瘍性増殖とアポトーシスによる退縮を来す．苺状血管腫(図1)と呼ばれてきた病変である．生後1～4週に出現し，1年以内に急速に増大する(増殖期)．その後90%以上の血管腫は5～7歳までに数年かけて徐々に自然消退する(退縮期，図2)．3～9：1の頻度で女性に多い．増生血管が皮内に限局する局面型(図1)，皮内から皮下組織まで広がる腫瘤型，および皮下組織に限局する皮下型(図2)があり，皮下型では血管奇形と混同されることが多い．乳児血管腫では増殖期，退縮期を通じてerythrocyte-type glucose transporter-1 (GLUT-1)免疫染色が陽性となるのに対し，血管奇形では陰性となる．

多くの血管腫は自然消退するため，経過観察のみで特に治療を必要としないが，整容目的でレーザー治療や切除が行われることもある．重要臓器の圧迫・機能低下・気道閉塞を生じる可能性がある病変，あるいは潰瘍・出血・心不全を来す病変に対しては，ステロイドの全身投与あるいは局注，インターフェロンの投与，塞栓術，切除術などが施行される．

b. 先天性血管腫(congenital hemangioma)

非常に稀な血管腫であり，rapidly involuting congenital hemangioma (RICH)とnoninvoluting congenital hemangioma (NICH)が含まれ，両者とも生下時に完成している[4) 5)]．RICHと乳児血管腫はともに退縮するが，RICHは生後約1年の間に急速に退縮することが特徴である．これに対しNICHは退縮しない[6)]．(図3)．発生頻度に性差はない．画像診断上，乳児血管腫との鑑別は困難である．病理学的には乳児血管腫がGLUT-1陽性であるのに対し，RICHとNICHでは陰性である．潰瘍・出血・整容目的で治療が必要であれば，切除術が施行される．

c. カポジ様血管内皮腫(kaposiform hemangioendothelioma)および房状血管腫[tufted angioma (angioblastoma of Nakagawa)]

Kasabach-Merritt現象を来す血管性腫瘍として臨床的に重要である[7)]．静脈奇形における消費性凝固障害(consumption coagulopathy, localized intravascular coagulopathy；LIC)と鑑別を要する．詳細は別稿に譲る．

2) 血管奇形(vascular malformation)

血管奇形は発生学的には胎生4～10週の末梢血管系形成期の異常によって生じ，その構成成分から，静脈奇形，動静脈奇形，リンパ管奇形，および毛細血管奇形などに分類され，その混合型も存在する(図4)[8)]．

図5 静脈奇形
A：胸部から左上肢の腫脹が見られ，皮膚は青色の色調を呈する．
B：筋肉内，皮下に静脈奇形が見られ，著明な高信号を呈している．

発生頻度に性差はなく，成長期などにゆっくりと増大し，退縮しない．

a. 静脈奇形（venous malformation）

静脈奇形は筋層外皮の低形成を来し拡張した静脈腔で構成される．従来，海綿状血管腫，筋肉内血管腫と呼ばれてきた病変は静脈奇形である．周囲組織の圧迫，血栓形成による疼痛や機能障害を生じることがある．頭頸部病変などでは腫脹による整容的な問題が生じる．その他，重要な病態として消費性凝固障害，下肢深部静脈血栓症・肺塞栓症を来すことがある．

静脈奇形は皮下にあれば青色～紫色を呈し，下垂，鬱血により腫脹し，挙上，圧迫により縮小する．拍動，血管雑音は見られない（図5）．

静脈奇形の保存的治療には，疼痛や腫脹に対して弾性衣類による圧迫が用いられる．疼痛・機能障害を有するか，経過観察で急速に増大する病変に対して，あるいは整容目的で，従来手術が行われてきたが，近年硬化療法が手術に取って代わる治療になりつつある．

b. 動静脈奇形（arteriovenous malformation）

動静脈奇形は動脈と静脈が正常の毛細血管床を介さずに，異常な交通を生じた先天性の病変である．動静脈奇形の臨床症状はSchöbinger分類（表3）[9]で示すとおり，疼痛，腫脹，潰瘍，出血を来し，大きな病変では心不全を来すことがある．皮膚は温かく，拍動，血管雑音がある（図6）．

表3 動静脈奇形のSchöbinger分類

病期	症状
I 静止期	皮膚紅潮，温感
II 拡張期	血管雑音，拍動音の聴取，増大
III 破壊期	疼痛，潰瘍，出血，感染
IV 代償不全期	心不全

（文献9）より転載）

動静脈奇形の保存的治療として，四肢病変では，静脈圧上昇による疼痛や腫脹に対して，弾性衣類による圧迫が用いられる．動静脈奇形の積極的な治療としては手術や塞栓術・硬化療法があるが，適応・方法はいまだ確立されていない．

c. リンパ管奇形（lymphatic malformation）

リンパ管の形成不全であり，胎生期の未熟リンパ組織がリンパ管に接合できずに，孤立して嚢腫状に拡張した病変と考えられている．リンパ管腫と呼ばれてきた病変である．microcystic（従来のlymphangioma），macrocystic（従来のcystic hygroma）に

A　肉眼所見

図6　動静脈奇形
A：手背に屈曲蛇行する血管が見られ，手指に腫脹，pseudo Kaposi sarcomaと呼ばれる皮膚病変（動静脈奇形で見られる皮膚病変）が見られる．
B，C：拡張蛇行する動脈（→），動静脈短絡（➤），拡張した流出静脈（➤）が見られる．

B　前腕動脈造影像（動脈早期相）

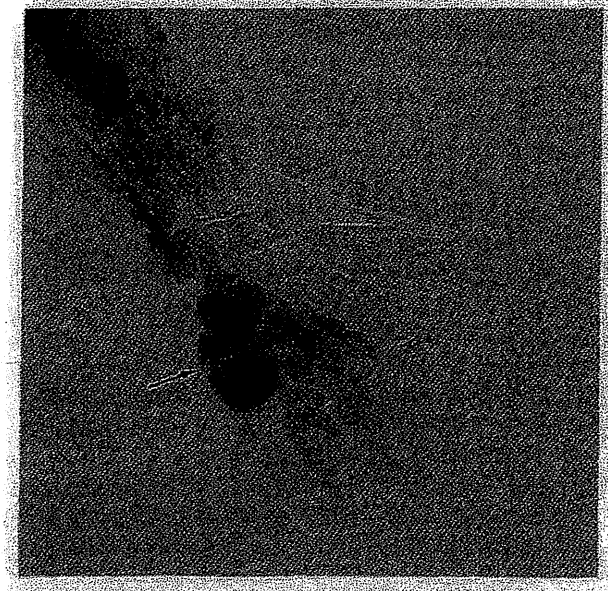

C　前腕動脈造影像（動脈後期相）

肉眼所見

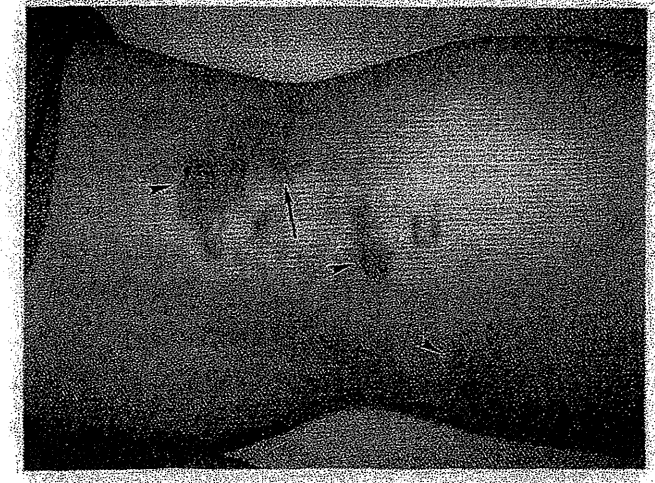

図7　リンパ管奇形
水疱が集簇した蛙の卵状の皮膚病変（→）で，出血を伴うと紫色を呈する（➤）．

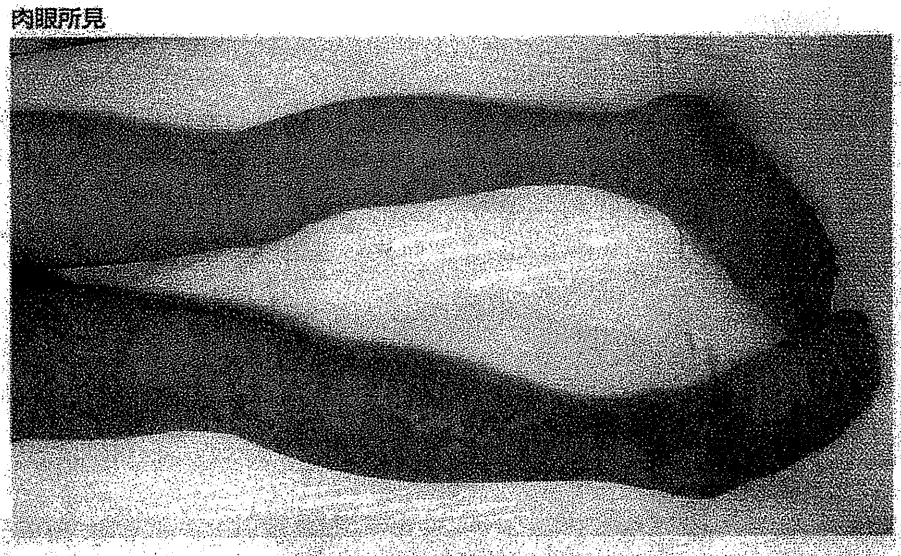

図8　毛細血管奇形
いわゆるポートワイン斑である.

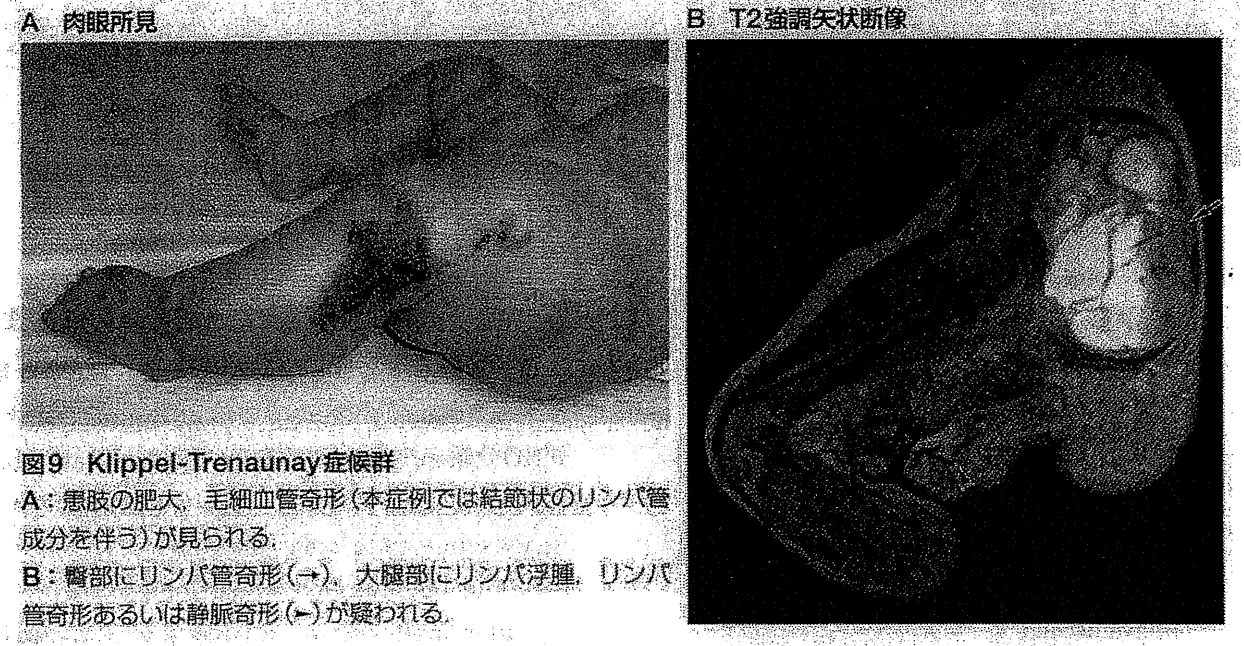

図9　Klippel-Trenaunay症候群
A：患肢の肥大，毛細血管奇形（本症例では結節状のリンパ管成分を伴う）が見られる.
B：臀部にリンパ管奇形（→），大腿部にリンパ浮腫，リンパ管奇形あるいは静脈奇形（←）が疑われる.

分類される．しばしば炎症を伴い，一時的に増大し，腫脹・発赤・熱感・疼痛を来す．真皮病変は典型的には粟粒大の水疱が集簇した病変であり（図7），皮下病変は多房性あるいは単房性嚢胞性腫瘤として認められる．保存的治療としては炎症を来した際に抗菌薬，抗炎症薬が投与される．積極的治療としては硬化療法・切除術が行われる.

なお，乳児血管腫に相当するリンパ管病変（リンパ管腫）の存在を支持する意見があるが，ISSVA分類では記載されていない.

d. 毛細血管奇形（capillary malformation）

皮膚の毛細血管拡張による赤色～暗赤色の色素斑であり，顔面・体幹部に好発する．単純性血管腫，ポートワイン斑と呼ばれてきた病変である（図8）．整容目的の治療が主となり，積極的治療としてはレーザー治療・切除が行われる．皮膚病変であり，一般に画像診断や血管内治療の適応とはならない.

e. 混合型（複合型）血管奇形（combined vascular malformation）

種々の混合型血管奇形があるが，患肢の肥大を伴う代表的な病変として，slow-flowのKlippel-Trenaunay症候群（CVM, CLVM）（図9），fast-flowのParkes Weber症候群（CAVM, CAVLM）（図10）が挙げられる．詳細は別稿に譲る.